Asociación Argentina
de Mecánica Computacional

Mecánica Computacional Vol XXV, pp. 1927-1946
Alberto Cardona, Norberto Nigro, Victorio Sonzogni, Mario Storti. (Eds.)
Santa Fe, Argentina, Noviembre 2006

# NUMERICAL SIMULATION OF LARGE STRAIN RATE DEPENDENT J2 PROBLEMS.

**Carlos García Garino[a,b], Jean-Philippe Ponthot[c], Anibal Mirasso[a,d], Roxane Koeune[c], Pierre-Paul Jeunechamps[c] and Claudio Careglio[a]**

[a]*LAPIC, Instituto Tecnológico Universitario, Universidad Nacional de Cuyo Casilla de Correo 947, 5500 Mendoza, Argentina. e-mail: cgarcia@itu.uncu.edu.ar, ccareglio@uncu.edu.ar*
[b]*Miembro de la Carrera del Investigador de CONICET*
[c]*LTAS-Aerospace and Mechanics, Université de Liège, Belgium e-mail: {JP.Ponthot,R.Koeune,ppjeunechamps}@ulg.ac.be*
[d]*Facultad de Ingeniería, Universidad Nacional de Cuyo, Centro Universitario, Parque San Martín, 5500 Mendoza, Argentina e-mail: aemirasso@uncu.edu.ar*

**Keywords:** Viscoplasticity, large strains, numerical simulation.

**Abstract.** This paper discusses a constitutive model for large strain viscoplasticity implemented in a model based on hyperelasticity. Viscoplasticity is derived in the context of Perzyna model, based on an extended yield criteria proposed originally by Ponthot. In the paper details of large strain viscoplastic model based on hypoelasticity, implemented in the code Metafor, are presented for comparison purposes. The hyperelastic large strain model extended to viscoplasticity has been implemented in Sogde following a previous work of the authors. Numerical problems in small strain case as well as large strain conditions have been tested. Viscoplastic solutions recover limit elastic and elastoplastic cases with both codes. The results obtained with both codes are practically identical for the small strain problem tested. For the large strain case both codes agrees well for limiting cases, but some differences in the load level attained for intermediate values of viscosity are found.

Copyright © 2006 Asociación Argentina de Mecánica Computacional http://www.amcaonline.org.ar

## 1 INTRODUCTION

In this paper the derivation of a large strain viscoplastic model based on hyperelasticity, based on a previous work of the authors (Ponthot et al., 2005) is discussed. The large strain model structure is taken from previous work of García-Garino (1993); Garino and Oliver (1995, 1996), derived in the context of the ideas of Simó (1988a,b); Simó and Ortiz (1985) for the rate independent case. A viscoplastic Perzyna type model is implemented following a work of Ponthot (2002) where a unified algorithm for elasto/viscoplastic problems has been proposed.

The kinematics of the resultant constitutive model is based on the multiplicative decomposition of deformation gradient tensor (Lee, 1969). Stresses can be derived from a hyperelastic potential and the model is written in the framework of internal variables theory and thermodynamics of irreversible solids (Lubliner, 1990). The stress update algorithm proposed by Ponthot treats the elasto/viscoplastic problem in a unified way. For a J2-flow material model, it is a simple generalization to rate-dependent problems of the radial return algorithm for rate-independent plasticity, including a generalized consistency condition. The resultant numerical model has been implemented and tested in the code Sogde.

In the paper the main ideas of a similar constitutive model proposed by Ponthot (2002) are discussed in order to provide a framework for the discussion of results obtained with Sogde and Metafor, a code where a model due to Ponthot has been implemented.

The classical *elastic* predictor - *plastic* corrector split problem is used in the numerical scheme of both codes tested. In this way a fully implicit algorithm is designed. The resultant update algorithm is written in terms of kinematics quantities instead of the usual one defined for the stress tensor. In the work it is shown that the unified elasto/viscoplastic stress update proposed by Ponthot (2002) is naturally included in the (previous) numerical structure of rate independent case, as regards the update be rewritten in terms of kinematic variables.

In a previous work of the authors (Ponthot et al., 2005) a list of references were suggested in order to review the state of the art of the problem. A comprehensive account of the problem can be found in the textbooks of Lubliner (1990), for the fundamentals, and Ottosen and Ristinmaa (2005) both for theory and numerical discussion. In the works of Perzyna (1966, 1971) distinctive features of so called Perzyna models of viscoplasticity can be found.

An overview of numerical algorithms proposed for viscoplasticty can be seen in the work of Ponthot (2002) and references therein. Many different algorithms have been developed in order to integrate elastic-viscoplastic equations, and a valuable discussion can be found in Golinval (1988). In general the models proposed in the literature, see for instance Hughes and Taylor (1978), Suliciu (1998), Pan (1997), Rubin (1996), Bruhns and Rott (1994) among others, in general don't exhibit the same level of performance as the radial return algorithm for plasticity.

Rather few works for rate dependent Perzyna models are discussed in the framework of large strain models. Wang and Sluys (2000) have proposed an incremental model for the elastic problem and the integration of the problem is carried out using a midpoint rule. Ponthot (2002) has proposed model based on hypoelasticty for the elastic problem and viscoplastic effects are integrated with a unified (plastic/viscoplastic) stress update procedure. Simo and Hughes (1998) have discussed the problem for a Duvaut-Lyons model type. Carosio et al. (2000); Carosio (2001) proposed a unified analysis for the problem, denoting the model of Ponthot (2002) as continuum viscoplasticty and the one due to Wang and Sluys (2000) as consistent viscoplasticity. However the comparison of this model has been formulated only for small strain problems. Alfano et al. (2001) presented general solución procededures in elasto/viscoplasticity for the small strain case too.

Copyright © 2006 Asociación Argentina de Mecánica Computacional http://www.amcaonline.org.ar

In section 2 of the work some results of the large strain kinematics are provided in order to provide some tools for the derivation of theoretical models, carried out in section 3 for large strain elasticity and in section 4 for viscoplasticity. Then numerical algorithms are discussed in section 5 and the results obtained with the two codes tested are discussed in section 6, in order to provide conclusions of the work.

## 2 KINEMATICS

In order to describe the kinematics of a solid under large deformation two configurations of a body are considered. The first one, usually konwn as reference configuration (not necessarily the initial configuration) at a certain time $t_0$ is denoted as ${}^o\Omega$, where the position of a material particle at this time is denoted by its position vector $\boldsymbol{X}$. The second configuration considered is the current or deformed configuration, at time $t$, denoted as ${}^t\Omega$, where the position of the same material particle is $\boldsymbol{x}$. In figure 1 both configurations are shown. There exists an equation that relates the position of material particle in both configurations $\boldsymbol{X}$ and $\boldsymbol{x}$ respectively, of the form:

$$\boldsymbol{x} = \boldsymbol{x}(\boldsymbol{X}, t) \tag{1}$$

The velocity of the reference point $\boldsymbol{X}$ is the material time derivative of the position vector and is defined by

$$\boldsymbol{v} = \dot{\boldsymbol{x}} = \frac{\partial\, \boldsymbol{x}(\boldsymbol{X}, t)}{\partial\, t} \tag{2}$$

The *d*eformation gradient of the motion at $\boldsymbol{X}$ is the second-rank two-point tensor $\boldsymbol{F}$ such that

$$\boldsymbol{F} = \frac{\partial\, \boldsymbol{x}}{\partial\, \boldsymbol{X}} \qquad \text{with} \qquad J = \det \boldsymbol{F} > 0 \tag{3}$$

By the polar decomposition, we can uniquely decompose $\boldsymbol{F}$ as

$$\boldsymbol{F} = \boldsymbol{R}\boldsymbol{U} \qquad \text{with} \qquad \boldsymbol{R}^T\boldsymbol{R} = \boldsymbol{I} \qquad \text{and} \qquad \boldsymbol{U} = \boldsymbol{U}^T \tag{4}$$

The corresponding *s*patial gradient of velocity is given by

$$\boldsymbol{l} = \frac{\partial\, \boldsymbol{v}}{\partial\, \boldsymbol{x}} = \dot{\boldsymbol{F}}\boldsymbol{F}^{-1} \tag{5}$$

It can be decomposed into a symmetric and antisymmetric part, $\boldsymbol{l} = \boldsymbol{d} + \boldsymbol{w}$ with

$$\boldsymbol{d} = \tfrac{1}{2}\,(\boldsymbol{l} + \boldsymbol{l}^T) \qquad \text{the rate of deformation} \tag{6}$$

$$\boldsymbol{w} = \tfrac{1}{2}\,(\boldsymbol{l} - \boldsymbol{l}^T) \qquad \text{the spin tensor} \tag{7}$$

The Almansi strain tensor, that is a useful measure for large strain problems, is defined in the current configuration ${}^t\Omega$ as:

$$\boldsymbol{e} = \frac{1}{2}(\boldsymbol{g} - \boldsymbol{b}^{-1}) \tag{8}$$

where $\boldsymbol{g}$ is the spatial metric tensor, and $\boldsymbol{b}^{-1} = \boldsymbol{F}^{-T}\boldsymbol{F}^{-1}$ is the Finger tensor.

For the elastoplastic continuum the kinematics of the problem can be extended on the basis of the very well known multiplicative decomposition of deformation gradient tensor $\boldsymbol{F}$ in its

Copyright © 2006 Asociación Argentina de Mecánica Computacional http://www.amcaonline.org.ar

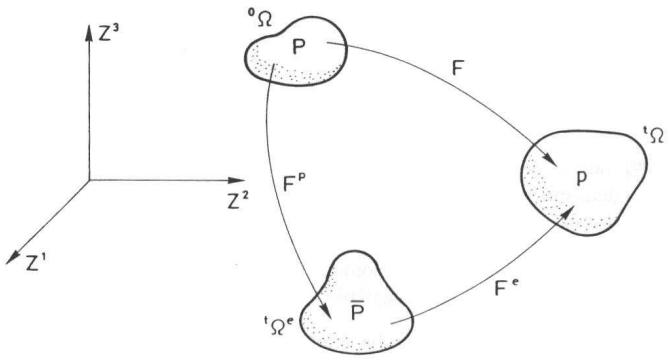


Figure 1: Kinematics of large strain elastoplastic solid: configurations

elastic and plastic components (Lee, 1969), as is it shown in equation (9) and illustrated in figure 1.

$$\boldsymbol{F} = \boldsymbol{F}^e \, \boldsymbol{F}^p \tag{9}$$

From equation (9) can be derived additive decompositions for Almansi strain tensor and rate of deformation tensor as can be seen in eq. (10) and (11) respectively.

$$\boldsymbol{e} = \boldsymbol{e}^e + \boldsymbol{e}^p \tag{10}$$

$$\boldsymbol{d} = \boldsymbol{d}^e + \boldsymbol{d}^p \tag{11}$$

where $\boldsymbol{e}^e$ and $\boldsymbol{e}^p$ tensors are defined as the Almansi strain tensor $\boldsymbol{e}$, but replacing $\boldsymbol{F}$ for $\boldsymbol{F}^e$ and $\boldsymbol{F}^p$ respectively. From the literature can be recognized that eq. (11) is the Lie derivative $L_v$ (Marsden and Hughes, 1983) of eq. (10).

## 3 LARGE STRAIN ELASTIC CONSTITUTIVE MODELS

In this section hyperelastic and hypoelastic models are introduced. The hypoelastic models were during many years the classical option in computational mechanics literature but since the late years of the eighties hyperelastic models become a valuable alternative.

### 3.1 Hypoelastic Constitutive Models

A Hypoelastic Constitutive model can be defined as linear relation between an objective derivative of Cauchy stress tensor $\boldsymbol{\sigma}$ and the rate of deformation tensor $\boldsymbol{d}$, by mean of fourth order constant tensor $\boldsymbol{D}$(Truesdell and Noll, 1965).

$$\overset{\triangledown}{\sigma}_{ij} = D_{ijkl} d_{kl} \qquad \text{or} \qquad \overset{\triangledown}{\boldsymbol{\sigma}} = \boldsymbol{D} : \boldsymbol{d} \tag{12}$$

where $\boldsymbol{D}$ is the Hooke stress-strain tensor given by

$$\boldsymbol{D}_{ijkl} = K \, \delta_{ij}\delta_{kl} + 2G \, (\delta_{ik}\delta_{jl} - \frac{1}{3}\delta_{ij}\delta_{kl}) \tag{13}$$

In the case of an elastoplastic material the stress depends on the elastic component $\boldsymbol{d}^e$ of rate of deformation tensor.

One of the major challenges while integrating the rate equation (12) in large-deformation analysis is to achieve incremental objectivity i.e. to maintain correct rotational transformation

Copyright © 2006 Asociación Argentina de Mecánica Computacional http://www.amcaonline.org.ar

properties all along a finite time step. However, standard time-discretization procedures, when applied to objective rate constitutive equations, typically only achieve objectivity in the limit of vanishingly small time steps. In order to overcome that problem, a procedure that has now become very popular, is to rewrite the equations in a corotational moving frame.

For a given group of rotations $\rho$ , it is possible to generate a change of frame from the fixed Cartesian reference axes to the corresponding rotating axes (corotational axes). In these axes, when transformed by $\boldsymbol{\rho}$, the Cauchy stress $\boldsymbol{\sigma}$ becomes

$$\boldsymbol{\sigma}^c = \boldsymbol{\rho}^T \boldsymbol{\sigma} \boldsymbol{\rho} \tag{14}$$

and upon time differentiation of this expression results:

$$\dot{\boldsymbol{\sigma}}^c = \boldsymbol{\rho}^T (\dot{\boldsymbol{\sigma}} - \boldsymbol{\omega}\boldsymbol{\sigma} + \boldsymbol{\sigma}\boldsymbol{\omega})\boldsymbol{\rho} = \boldsymbol{\rho}^T \overset{\nabla c}{\boldsymbol{\sigma}} \boldsymbol{\rho} \tag{15}$$

where $\overset{\nabla c}{\boldsymbol{\sigma}}$ is a corotational objective stress rate e.g.

$\overset{\nabla c}{\boldsymbol{\sigma}}$ is Jaumann rate if $\boldsymbol{\omega} = \boldsymbol{W}$

$\overset{\nabla c}{\boldsymbol{\sigma}}$ is Green-Naghdi rate if $\boldsymbol{\omega} = \dot{\boldsymbol{R}}\boldsymbol{R}^T$

Expression (15) indicates that, a somewhat complicated expression as an objective derivative becomes a rather simple time derivative under the appropriate change of coordinates. This suggests that the entire theory and implementation will take on canonically simpler forms if transformed to the $\boldsymbol{\rho} - system$. For more details on this change of coordinate, see Ponthot (1995) and Hughes (1983). In the new reference frame, the evolution equation take the simpler form:

$$\dot{\boldsymbol{\sigma}}^c = \boldsymbol{D}^c : \boldsymbol{d}^c \tag{16}$$

### 3.2 Hyperelastic Constitutive Models

These models are defined from a free energy function $\psi$ that plays the role of an elastic potential. The Cauchy stresses can be derived as shown in eq. (17).

$$\boldsymbol{\sigma} = \frac{\partial \psi}{\partial \boldsymbol{e}} \tag{17}$$

In practice, it is possible for metals to write free energy function as a quadratic function of Almansi strain tensor $\boldsymbol{e}$ and material constants $\lambda$ and $\mu$ as it is shown in equation (18).

$$\psi^e = \left[ \frac{1}{2} \lambda \, tr(\boldsymbol{e})^2 \; + \; \mu \, (\boldsymbol{e} : \boldsymbol{e}) \right] \tag{18}$$

From equation (17) the Cauchy stress tensor results:

$$\boldsymbol{\sigma} = \lambda \, tr(\boldsymbol{e}) \, \mathbf{1} \; + \; 2 \, \mu \, \boldsymbol{e} \tag{19}$$

This model has been used previously by García-Garino (1993); Garino and Oliver (1995, 1996) as an alternative to the neohookean models proposed by another authors (Simó, 1988a,b; Simó and Ortiz, 1985). The fourth order tensor $\boldsymbol{D}$ defined in eq. (13) can be recovered in this case as $\dfrac{\partial \boldsymbol{\sigma}}{\partial \boldsymbol{e}}$.

Copyright © 2006 Asociación Argentina de Mecánica Computacional http://www.amcaonline.org.ar

### 3.3 Comparison of Hypoelastic and Hyperelastic Models

For large strain regimen the hyperelastic and hypoelastic constitutive models, given in equations (12) and (19) respectively, define different materials if the same fourth order constitutive tensor is used in both models. In order to ilustrate this point, the analytical response of both models under a uniaxial extension are given in equations (20) and (21), respectively (see García-Garino (1993), appendix 1, AnI.6.1). For both models material constants $\lambda = 1$ and $\mu = 1$ are considered.

$$\boldsymbol{\sigma}(t) = \frac{1}{2}(\lambda + 2\mu)\frac{(1+t^2)-1}{(1+t)^2} \tag{20}$$

$$\boldsymbol{\sigma}(t) = (\lambda + 2\mu)t \tag{21}$$

The response of both model is compared in Figure 2 for a large extension (left) and small strain case (right).

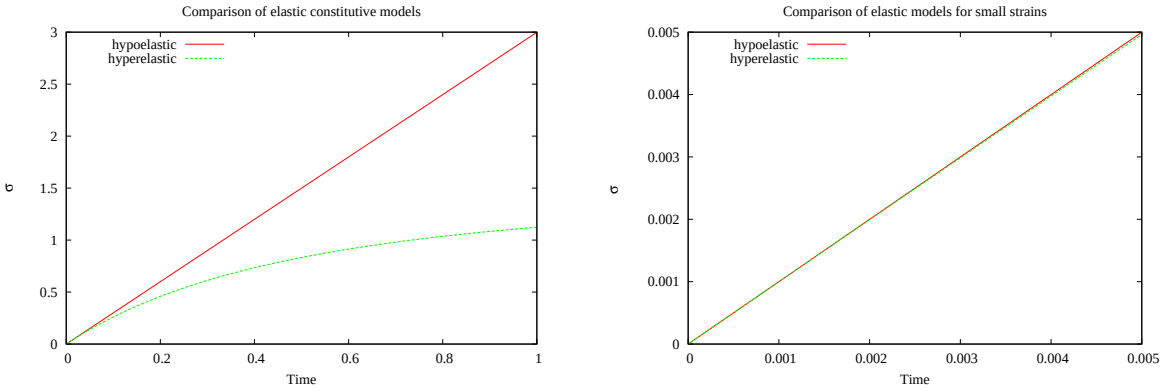


Figure 2: *Large strain models comparison*

REMARKS

1. For large displacements but small deformations problems, like elastic buckling and other applications usually found in structural analysis, both model show the same response.

2. In presence of large deformation but small elastic strains, like in metal forming applications, practially the same results are obtained with the discussed models. See (García-Garino, 1993) and (Ponthot, 1995) for available comparisons.

3. Different responses can be expected when elastic deformations are large or moderate.

## 4 LARGE STRAIN VISCOPLASTIC MODEL

In this section viscoplastic problem is presented and the distinctive features (Perzyna, 1966, 1971) are briefly introduced. The main results of J2 rate independent case are first presented in order to provide a framework for the discussion of viscoplasticity.

Copyright © 2006 Asociación Argentina de Mecánica Computacional http://www.amcaonline.org.ar

### 4.1 Rate Independent J2 model

Plasticity is taken into account by means of an associative flow rule $f = g$, where $f$ and $g$ accounts for the yield and plastic potential functions respectively. The yield function is the very well known Von Mises or J2 model given in equation (22).

$$f(\boldsymbol{\sigma}, \sigma_y) = \bar{\sigma} - \sigma_y = 0 \tag{22}$$

where $\bar{\sigma} = \sqrt{\frac{3}{2}\boldsymbol{s} : \boldsymbol{s}}$ denotes equivalent stress, $\boldsymbol{s}$ is the deviatoric stress tensor and $\sigma_y$ is the current yield stress.

Flow rule can be written now in terms of yield criteria $f$ as:

$$\boldsymbol{d}^p = \dot{\gamma} \quad \boldsymbol{n} \qquad \text{where} \qquad n_{ij} = \frac{s_{ij}}{\sqrt{s_{kl}s_{kl}}} \tag{23}$$

$\boldsymbol{n}$ denotes the unit outward normal to the yield function ($\boldsymbol{n} : \boldsymbol{n} = 1$) to the yield surface and $\gamma$ is the plastic multiplier.

The plastic multiplier $\gamma$ can be computed from the consistency condition, obtained after time differentation of the yield function $f$.

$$\dot{f}(\boldsymbol{\sigma}, \sigma_y) = 0 \tag{24}$$

The loading/unloading conditions can be obtained from the Kuhn-Tucker inequalities:

$$\gamma f = 0, \qquad \gamma \geq 0, \qquad f \leq 0 \tag{25}$$

The hardening law that brings the evolution law of yield stress $\sigma_y$ is written in terms of proper internal variables. In this work only linear isotropic hardening is considered.

$$\dot{\sigma_y} = h\dot{\bar{\epsilon}}^p \tag{26}$$

where $h$ is a material parameter that corresponds to the slope of the effective stress vs. effective plastic strain curve under uniaxial loading conditions, also known as hardening module in the case linear hardening. The effective plastic strain $\dot{\bar{\epsilon}}^p$ can be computed from the plastic flow as:

$$\dot{\bar{\epsilon}}^p = \sqrt{\frac{2}{3}\boldsymbol{d}^p : \boldsymbol{d}^p} = \sqrt{\frac{2}{3}}\dot{\gamma} \tag{27}$$

### 4.2 Perzyna J2 viscoplastic model

The kinematics of the problem can be generalised for the viscoplastic problem as shown in equations (28) and (29).

$$\boldsymbol{e} = \boldsymbol{e}^e + \boldsymbol{e}^{vp} \tag{28}$$

$$\boldsymbol{d} = \boldsymbol{d}^e + \boldsymbol{d}^{vp} \tag{29}$$

where $\boldsymbol{e}^{vp}$ and $\boldsymbol{d}^{vp}$ are viscous counterpart of plastic components of Almansi strain tensor $\boldsymbol{e}^p$ and rate of deformation tensor $\boldsymbol{d}^p$ respectively.

Contrary to the case of rate independent plasticity, the effective stress $\bar{\sigma}$ is no longer constrained to remain less or equal to the yield stress but one can have $\bar{\sigma} \geq \sigma_y$ . Therefore the *overstress* $d$ is defined as:

$$d = \langle \bar{\sigma} - \sigma_y \rangle \tag{30}$$

Copyright © 2006 Asociación Argentina de Mecánica Computacional http://www.amcaonline.org.ar

where $\langle x \rangle$ denotes the Mac Auley brackets defined by $\langle x \rangle = 1/2(x + |x|)$. Clearly, an inelastic process can only take place if, and only if, the overstress $d$ is positive, consequently $f \geq 0$.

For this problem Perzyna (1966, 1971) proposed the following flow rule:

$$\boldsymbol{d}^{vp} = \langle \phi(d, \eta) \rangle \, \boldsymbol{n} \tag{31}$$

where $\eta$ is the viscosity of the material. Many alternatives has been proposed in practice in order to generalize the function $\phi(d, \eta)$.

The structure of viscoplastic flow given in equation (31) suggests that function $\phi$ plays the role of a *viscoplastic parameter* $\gamma^{vp}$. In this sense this kind of models can be considered as penalty regularization of rate-independent plasticity where the consistency parameter has been replaced by an increasing function of the overstress like the one proposed by Ponthot (2002):

$$\dot{\gamma}^{vp} = \sqrt{\frac{3}{2}} \left\langle \frac{\bar{\sigma} - \sigma_y}{\eta (\bar{\epsilon}^{vp})^{1/n}} \right\rangle^m \tag{32}$$

where $n$ is a hardening exponent, $m$ is a rate sensitivity parameter and $\bar{\epsilon}^{vp}$ is the equivalent viscoplastic flow. Taking into account equations (31) and (32) the viscoplastic flow can be expressed in a similar way to the rate independent problem as:

$$\boldsymbol{d}^{vp} = \dot{\gamma}^{vp} \boldsymbol{n} \tag{33}$$

the equivalent equivalent viscoplastic flow $\bar{\epsilon}^{vp}$ can be computed from (27) replacing $\boldsymbol{d}^p$ for $\boldsymbol{d}^{vp}$.

$$\bar{\epsilon}^{vp} = \sqrt{\frac{2}{3} \boldsymbol{d}^{vp} : \boldsymbol{d}^{vp}} = \sqrt{\frac{2}{3}} \dot{\gamma} \tag{34}$$

In this problem the hardening law given in (26) is valid providing $\bar{\epsilon}^{vp}$ be the internal variable.

From equations (34) and (32) results:

$$\bar{\epsilon}^{vp} = \sqrt{\frac{2}{3}} \dot{\gamma}^{vp} = \left\langle \frac{\bar{\sigma} - \sigma_y}{\eta (\bar{\epsilon}^{vp})^{1/n}} \right\rangle^m \tag{35}$$

so that, in the viscoplastic range, a new constraint is defined (Ponthot, 2002).

$$\bar{f} = \bar{\sigma} - \sigma_y - \eta (\bar{\epsilon}^{vp})^{1/n} (\dot{\bar{\epsilon}}^{vp})^{1/m} = 0 \tag{36}$$

This criterion is a *generalization of the classical von-Mises criterion $f = 0$ for rate-dependent materials*. The latter can simply be recovered by imposing $\eta = 0$ (no viscosity effect). On the other hand if a large enough value is adopted for $\eta$ the elastic response is recovered. Kuhn Tucker conditions can be written in a similar way to the rate independent case (see Ponthot (2002) for details).

$$\dot{\gamma}^{vp} \bar{f} = 0, \qquad \dot{\gamma}^{vp} \geq 0, \qquad \bar{f} \leq 0 \tag{37}$$

## 5 NUMERICAL SCHEME

In this section the numerical scheme necessary to implement the discussed theoretical model in a finite element code is introduced. This scheme is based on a predictor (*elastic*)-corrector *elasto/viscoplastic* technique. The predictor scheme is discussed in subsection 5.1, where the case of Metafor (Hypoelasticity) is discussed in paragraph 5.1.1, and the predictor problem for for Sogde (Hyperelasticity) can be seen in paragraph 5.1.2. The viscoplastic corrector is written in terms of stress in Metafor and in function of strains in Sogde. However after a previous work of the authors (Ponthot et al., 2005) the problem can be presented in a unified format.

Copyright © 2006 Asociación Argentina de Mecánica Computacional http://www.amcaonline.org.ar

### 5.1 Elastic Problem

#### 5.1.1 Predictor for the hypoelastic model

In this section the numerical scheme in order to compute the trial stress are briefly reviewed following the ideas of Ponthot (2002), where a detailed derivation of the scheme can be found.

In the corotational frame, the equation to integrate simply reduces to

$$\dot{\boldsymbol{\sigma}}^c = \boldsymbol{D} : \boldsymbol{d}^c \tag{38}$$

In order to compute the trial stress tensor in corotational configuration the stress tensor ${}^t\sigma$ in the cartensian frame can be rewritten as:

$${}^t\boldsymbol{\sigma}^c = {}^t\boldsymbol{\rho}^T \, {}^t\boldsymbol{\sigma} \, {}^t\boldsymbol{\rho} \tag{39}$$

so that the trial elastic stress is given by :

$${}^{t+\Delta t}\boldsymbol{\sigma}^{c^{tr}} = {}^t\boldsymbol{\sigma}^c + \int_t^{t+\Delta t} \boldsymbol{D} : \boldsymbol{d}^c \, dt \tag{40}$$

or, in the Cartesian frame, for a constant elastic tensor $\boldsymbol{D}$, results :

$${}^{t+\Delta t}\boldsymbol{\sigma}^{tr} = {}^{t+\Delta t}\boldsymbol{\rho} \, {}^{t+\Delta t}\boldsymbol{\sigma}^{c^{tr}} \, {}^{t+\Delta t}\boldsymbol{\rho}^T = {}^{t+\Delta t}\boldsymbol{\rho} \left[ {}^t\boldsymbol{\rho}^T \, {}^t\boldsymbol{\sigma} \, {}^t\boldsymbol{\rho} + \boldsymbol{D} : \int_t^{t+\Delta t} \boldsymbol{D} : \boldsymbol{d}^c \, dt \right] {}^{t+\Delta t}\boldsymbol{\rho}^T \tag{41}$$

that can be understand, from a rather engineering point of view, like a three steps operation. If new operators $\rho^*$ and $\rho_*$ are introduced, that loosely accounts for *rotational* pull back and push forwards respectively, the algorithm can be expressed in compact form as can be seen in BOX 1.

BOX 1: Summary of predictor problem for hypoelastic model

For a given increment of time $\Delta t$ that maps configuration ${}^t\Omega$ in ${}^{t+\Delta t}\Omega$, tensors $\boldsymbol{\rho}$ and $\boldsymbol{d}^c$ computed from such mapping, and ${}^t\boldsymbol{\sigma}$ stored in data base of the problem, compute:

1. ${}^t\boldsymbol{\sigma}^c = {}^t\boldsymbol{\rho}^T \, {}^t\boldsymbol{\sigma} \, {}^t\boldsymbol{\rho}$, in compact form: ${}^t\boldsymbol{\sigma}^c = {}^t\rho^* \, {}^t\boldsymbol{\sigma}$
2. ${}^{t+\Delta t}\boldsymbol{\sigma}^{c^{tr}} = {}^t\boldsymbol{\sigma}^c + \int_t^{t+\Delta t} \boldsymbol{D} : \boldsymbol{d}^c \, dt$
3. ${}^{t+\Delta t}\boldsymbol{\sigma}^{tr} = {}^{t+\Delta t}\boldsymbol{\rho} \, {}^{t+\Delta t}\boldsymbol{\sigma}^{c^{tr}} \, {}^{t+\Delta t}\boldsymbol{\rho}^T$, in compact form: ${}^{t+\Delta t}\boldsymbol{\sigma}^{tr} = \rho_* \, {}^{t+\Delta t}\boldsymbol{\sigma}^{c^{tr}}$

In summary the trial stress in the final configuration can be written in compact form as:

$${}^{t+\Delta t}\boldsymbol{\sigma}^{tr} = \rho_* \left[ \rho^* \, {}^t\boldsymbol{\sigma} + \int_t^{t+\Delta t} \boldsymbol{D} : \boldsymbol{d}^c \, dt \right] \tag{42}$$

In order to simplify eq. (42) Ponthot (2002) suggested the following simplifficative assumptions:

1. The unrotated configuration is chosen as ${}^t\Omega$, then ${}^t\boldsymbol{\rho} = \boldsymbol{I}$

Copyright © 2006 Asociación Argentina de Mecánica Computacional http://www.amcaonline.org.ar

2. $\boldsymbol{\rho}(t) = \boldsymbol{R}$
3. $\boldsymbol{d}^e = \frac{\bar{\boldsymbol{C}}}{\Delta t}$, that comes from an exponential map for $\dot{\boldsymbol{U}}(t)$

the *incremental natural* strain tensor $\bar{\boldsymbol{C}}$ is defined as:

$$\bar{\boldsymbol{C}} = \ln \boldsymbol{U} = \frac{1}{2} \ln \boldsymbol{U}^2 = \frac{1}{2} \ln(\boldsymbol{F}^T \boldsymbol{F}) \tag{43}$$

Then the trial elastic stress can easily be computed as:

$$^{t+\Delta t}\boldsymbol{\sigma}^{tr} = {}^{t+\Delta t}\boldsymbol{R} \left[ {}^t\sigma + \boldsymbol{D} : \bar{\boldsymbol{C}} \right] {}^{t+\Delta t}\boldsymbol{R}^T = {}^{t+\Delta t}\boldsymbol{R} \left[ {}^t\sigma + \boldsymbol{D} : \ln(\boldsymbol{U}) \right] {}^{t+\Delta t}\boldsymbol{R}^T \tag{44}$$

### 5.1.2 Predictor for the hyperelastic model

In this problem the plastic quantities remain frozen: $({}^{t+\Delta t}\boldsymbol{F}^{pTR} = {}^t\boldsymbol{F}^p)$. The trial (*elastic*) component of the deformation gradient tensor results:

$$^{t+\Delta t}\boldsymbol{F}^{eTR} = {}^{t+\Delta t}\boldsymbol{F} \ \left({}^{t+\Delta t}\boldsymbol{F}^{pTR}\right)^{-1} = \boldsymbol{f} \ {}^t\boldsymbol{F} \ \left({}^t\boldsymbol{F}^p\right)^{-1} = \boldsymbol{f} \ {}^t\boldsymbol{F}^e \tag{45}$$

where $\boldsymbol{f}$ is the incremental deformation gradient tensor. The predictor value of the elastic Finger tensor ${}^{t+\Delta t}\boldsymbol{b}^{e-1^{TR}}$ is:

$$^{t+\Delta t}\boldsymbol{b}^{e-1^{TR}} = \left({}^{t+\Delta t}\boldsymbol{F}^{e-T} \ {}^{t+\Delta t}\boldsymbol{F}^{e-1}\right)^{TR} = \boldsymbol{f}^{-T} \ {}^t\boldsymbol{b}^{e-1} \ \boldsymbol{f}^{-1} \tag{46}$$

Finally, the trial stresses $\boldsymbol{\sigma}^{TR}$ are computed from eqn (46) in terms of the predictor value of elastic Almansi strain ${}^{t+\Delta t}\boldsymbol{e}^{eTR} = \frac{1}{2}({}^{t+\Delta t}\boldsymbol{g} - {}^{t+\Delta t}\boldsymbol{b}^{e-1^{TR}})$.

It is important to note that the elastic problem is reduced to the computation of a closed expression.

## 5.2 Viscoplastic Problem

In this case the geometry of body remains fixed and stress tensor and internal variables must be updated. The plastic corrector is derived first for the hyperelastic model following the ideas of a previous work of the authors (Ponthot et al., 2005). The flow rule given in eq. (31), can be written in the material configuration ${}^o\Omega$ in terms of the viscoplastic component of Right Cauchy Green tensor $\boldsymbol{C}^{vp}$ and viscoplastic multiplier $\lambda^{vp}$ as:

$$\dot{\boldsymbol{C}}^{vp} = 2 \ \phi^* \boldsymbol{d}^p = 2 \ \dot{\lambda}^{vp} \ \phi^* \boldsymbol{n} = 2 \ \dot{\lambda} \ \boldsymbol{N} \tag{47}$$

equation (47) is integrated using a Backward-Euler scheme:

$$^{t+\Delta t}\boldsymbol{C}^p - {}^t\boldsymbol{C}^p = 2 \ \lambda^{vp} \ {}^{t+\Delta t}\boldsymbol{N} \tag{48}$$

Following the same steps of the elastoplastic counterpart of this model García-Garino (1993); Garino and Oliver (1996) the updated Finger tensor results (Ponthot et al., 2005):

$$^{t+\Delta t}\boldsymbol{b}^{e-1} = {}^{t+\Delta t}\boldsymbol{b}^{e-1^{TR}} + 2 \ \lambda^{vp} \ {}^{t+\Delta t}\boldsymbol{n} \tag{49}$$

it is important to note that Finger tensor, and consequently stress tensor can be updated, once $\lambda^{vp}$ is computed. From definition of elastic component of Almansi strain tensor, see eq. (10), and eq. (49) results:

$$^{t+\Delta t}\boldsymbol{e}^e = \frac{1}{2} \left(g - {}^{t+\Delta t}\boldsymbol{b}^{e-1}\right) = \frac{1}{2} \left(g - {}^{t+\Delta t}\boldsymbol{b}^{e-1^{TR}} - 2 \ \lambda^{vp} \ {}^{t+\Delta t}\boldsymbol{n}\right) = {}^{t+\Delta t}\boldsymbol{e}^{eTR} - \lambda^{vp} \ {}^{t+\Delta t}\boldsymbol{n} \tag{50}$$

Copyright © 2006 Asociación Argentina de Mecánica Computacional http://www.amcaonline.org.ar

Introducing the viscoplastic correction of elastic component of Almansi strain tensor given in equation (50) in the constitutive equation (19), the corrector problem can be written in terms of stresses as:

$$^{t+\Delta t}\boldsymbol{\sigma} = {}^{t+\Delta t}\boldsymbol{\sigma}^{TR} \; - \; 2\,\lambda^{vp}\,\mu\,{}^{t+\Delta t}\boldsymbol{n} \tag{51}$$

that is the result shown in equation (51), section 6.3 in the work of Ponthot (2002), after integration over the time interval $[t, t+\Delta t]$, with initial conditions given by ${}^{t}\boldsymbol{\sigma}$, ${}^{t}\bar{\epsilon}^{vp}$ and ${}^{t}\sigma_y$. This result, found in a previous work of the authors (Ponthot et al. (2005)), shows that the hyperelastic model originally derived for elastoplastic problems naturally includes the viscous counterpart.

In order to compute the viscoplastic multiplier $\lambda^{vp}$ an integration procedure very similar to the radial return method of plasticity, proposed by Ponthot (2002) is used. The tensor ${}^{t+\Delta t}\boldsymbol{n}$ is approximated by:

$$^{t+\Delta t}\boldsymbol{n} = \frac{^{t+\Delta t}\boldsymbol{s}^{TR}}{\sqrt{^{t+\Delta t}\boldsymbol{s}^{TR} : {}^{t+\Delta t}\boldsymbol{s}^{TR}}} \tag{52}$$

so that the final values are given by

$$^{t+\Delta t}\bar{\epsilon}^{vp} \;=\; {}^{t}\bar{\epsilon}^{vp} + \sqrt{\frac{2}{3}}\lambda^{vp} \tag{53}$$

$$\dot{\bar{\epsilon}}^{vp} \;=\; \frac{^{t+\Delta t}\bar{\epsilon}^{vp} - {}^{t}\bar{\epsilon}^{vp}}{\Delta t} \tag{54}$$

where the (unknown) scalar parameter $\lambda^{vp}$ stands for

$$\lambda^{vp} = \int_t^{t+\Delta t} \dot{\lambda}\, dt \tag{55}$$

REMARK: It is important to point out that the first order approximation introduced in eq. (54) is fully consistent with the approximation introduced in eq. (48).

The $\lambda^{vp}$ parameter is simply determined by the enforcement of the *generalized consistency condition*, $\bar{f} = 0$, at time $t = t + \Delta t$, i.e.

$$\begin{aligned} \bar{f}(\lambda^{vp}) \;&=\; \sqrt{\frac{3}{2}\left[\boldsymbol{s}^{TR} - 2\mu\,\lambda^{vp}\,\boldsymbol{n}\right] : \left[\boldsymbol{s}^{TR} - 2\mu\,\lambda^{vp}\,\boldsymbol{n}\right]} - {}^{t+\Delta t}\sigma_y(\lambda^{vp}) \\ &-\; \eta\,(\bar{\epsilon}_0^{vp} + \sqrt{\frac{2}{3}}\lambda^{vp})^{\frac{1}{n}}\,(\sqrt{\frac{2}{3}}\frac{\lambda^{vp}}{\Delta t})^{\frac{1}{m}} = 0 \end{aligned} \tag{56}$$

where ${}^{t+\Delta t}\sigma_y$ is a given function of $\bar{\epsilon}^{vp}$ and consequently a given function of $\lambda^{vp}$.

The scalar equation (56) is a nonlinear expression where the only unknown parameter is $\lambda^{vp}$. It can be easily solved by a local Newton-Raphson iteration. In the particular case where $n = \infty$ (no multiplicative hardening), $m = 1$ (linear dependence between overstress and viscoplastic

Copyright © 2006 Asociación Argentina de Mecánica Computacional http://www.amcaonline.org.ar

rate of deformation), and $h =$ constant (linear hardening) a closed form solution of this equation is given by

$$\lambda^{vp} = \frac{1}{2\mu} \frac{\sqrt{\boldsymbol{s}^{TR} : \boldsymbol{s}^{TR}} - \sqrt{\frac{2}{3}} t \sigma_y}{1 + \frac{1}{3\mu}(h + \frac{\eta}{\Delta t})} \tag{57}$$

so that it is now obvious that the present algorithm is a generalization to the rate-dependent case of the classical radial return algorithm. This one is exactly recovered (with no numerical difficulty) by setting $\eta = 0$ (no viscosity effect). In the viscous case, one can see that the rate-dependent solution (57) is equivalent to rate-independent solution with a fictitious hardening given by $h^* = h + \eta/\Delta t$.

## 6 NUMERICAL SIMULATIONS

In this section numerical problems are simulated in order to compare the response of the two discussed models on one hand and to verify if the limit cases are numerically recovered. First a problem for small strain regimen is studied, in order to avoid the (possible) influence of non linear geometric effects in the obtained results. In a second case a problem nonlinear and material nonlinearities is carried out. In all cases Q1/P0 element is used.

### 6.1 Numerical simulation of a plane strain plate under small strain regime

In this problem, proposed by Alfano et al. (2001) a plane strain plate, with a central circular hole is studied. The dimensions of the plate are 18 x 10 m, R = 5 m. Material constants considered are: $E = 2.1\ 10^5$ Mpa; $\nu = 0.3$; $\sigma_y = 240$ Mpa; $H = 0$. A linear Perzyna viscoplastic model with $m = 1$ and $n = \infty$ is considered. Different viscosity values of $\eta$ parameter are taken studied: $10^2$, $10^{12}$ and $10^{15}$. In figure 3, the finite element mesh used is displayed. Imposed displacements (at y=18m) are applied until a final displacement of 50 mm is reached in 25 equals time steps.

In figure 4 load-displacements curves obtained with both codes can be seen. From the figure can be observed:

1. The elastic limit case is recoverd with both codes for a viscosity parameter $\eta = 10^{15}$.
2. The elastoplastic limit case is recovered with both codes for $\eta = \ 10^2$
3. Practically the same response is obtained with both codes for intermediate value of $\eta$, $10^{12}$.

From the results obtained can be said that both codes compares very well and the algorithm implemented represents properly the limit cases discussed in section 5.2.

It is worthwhile to note that both codes recover naturally small strain case, even when the respective models are derived for large strains situations. For the complete range of values of $\eta$ tested no difficulties for convergence were found.

### 6.2 Large strain simulation of a plane strain viscoplastic plate

The problem discussed in the previous section is studied again, but taking into account large strain regimen in this case. In order to reach large strains, a final displacement of 2000 mm is imposed. Metafor uses an automatic time step procedure that adjusts time step size based on the rate of convergence of previous iterations. In Sogde 400 equals time steps are considered in all cases, but larger increments can be fairly applied for elastic case and simulations with large

Copyright © 2006 Asociación Argentina de Mecánica Computacional http://www.amcaonline.org.ar

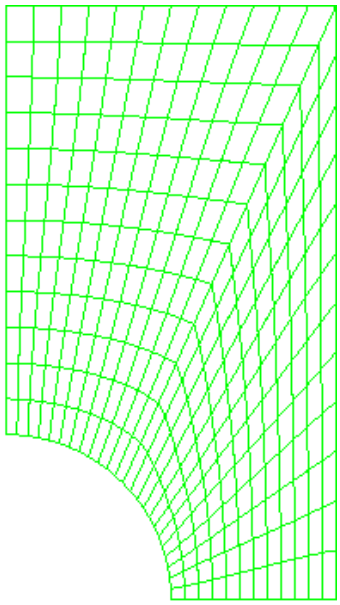

Figure 3: *Finite element mesh used for small strain simulations*

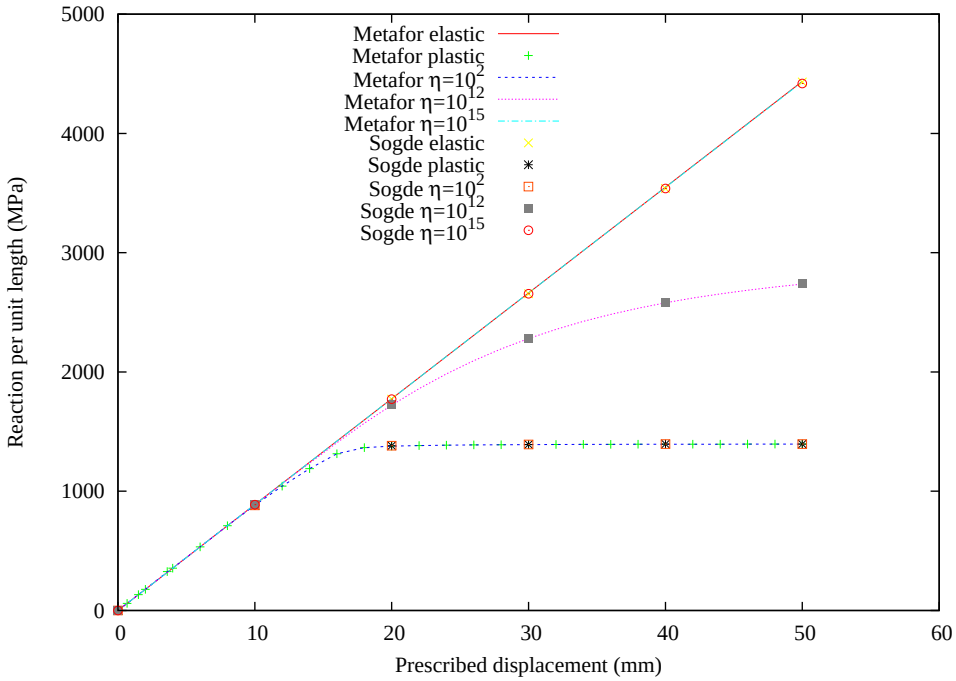


Figure 4: *Viscoplastic plane strain plate: load vs displacement history*

Copyright © 2006 Asociación Argentina de Mecánica Computacional http://www.amcaonline.org.ar

values of viscosity parameter $\eta$. The finite element mesh used in this case is the same to the small strain problem shown in 3.

In order to study the behaviour of both codes for limit elastoplastic case in figure 5 are shown the results obtained with Sogde and Metafor, for elastoplasticity and viscoplasticity with low viscosity parameter ( $\eta = 10^2$ and $\eta = 10^{15}$), in terms of load vs displacements histories.

From the figure can be seen:

1. The elastoplastic limit case is recoverd with both codes for a viscosity parameter $\eta = 10^2$.
2. For a viscosity parameter $\eta = 10^{10}$ the results tends to the elastoplastic solution. In this case similar solutions are found with Sogde and Metafor, but load level attained with Sogde is sligthy greater than Metafor.

It is important to point out that elastoplastic limit case is recovered for large strain case. On the other hand can be noted that the different elastic models considered in Metafor (hypoelasticity) and Sogde (hyperelasticity) does not affect the global results because the elastic strains remain small. This results confirm the good agreement obtained previously with this two codes for large strain elastoplastic problems (see Ponthot (1995) and García-Garino (1993).

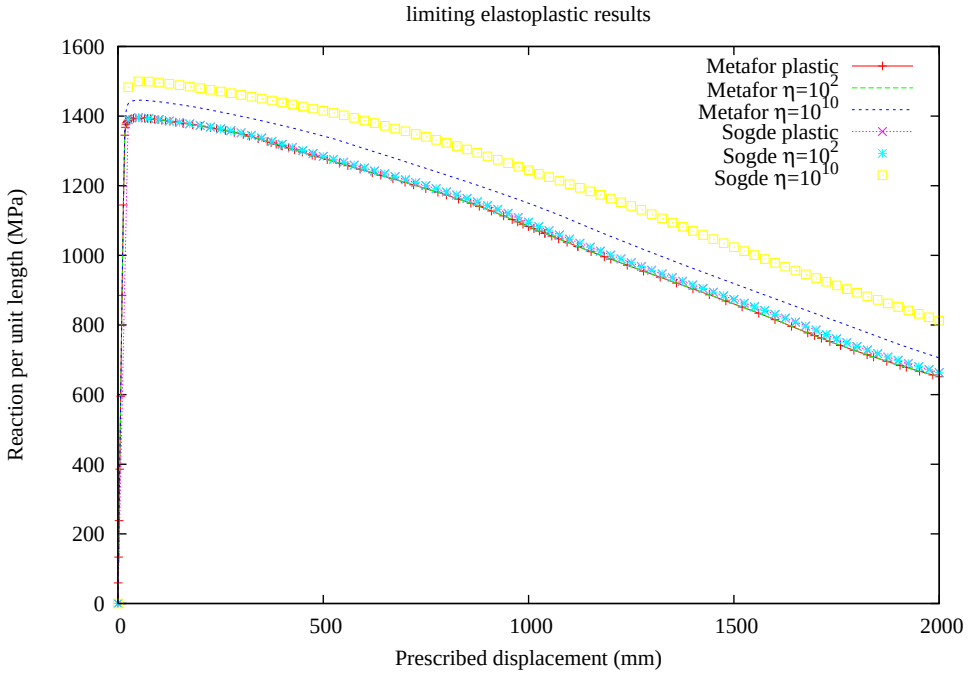


Figure 5: *load vs displacement histories for limiting elastoplastic case*

In all the cases tested in figure 5 a global softening behaviour is found, that can be explained from figure 9, where a comparison of deformed shapes is shown. For elastoplastic solution and viscoplastic cases with low viscosity parameters a strong reduction of the central section can be seen. For this case the response of the problem is a like *necking* case, and then a load reduction is obtained after the peak load. This effect, well known even for hardening materials, it is even more clear for non hardening materials like the one used in this case.

In figure 6 can be observed the results computed with Metafor and Sogde for elastic cases and viscoplastic solutions for large viscosity parameter ($\eta = 1.10^{15}$ and $\eta = 1.10^{17}$). Several considerations can be enuntiated:

Copyright © 2006 Asociación Argentina de Mecánica Computacional http://www.amcaonline.org.ar

1. The elastoplastic limit case is recoverd with both codes for a viscosity parameter $\eta = 10^{17}$.

2. For a viscosity parameter $\eta = 10^{15}$ the results tends to the elastic solution. In this case similar solutions are found with Sogde and Metafor, but load level attained with Sogde is sligthy smaller than Metafor.

In figure 6 can be seen that the elastic response computed with Metafor is practically linear, so agrees very well with the analytical model discussed in paragraph 3.3 and the curve obtained with Sogde presents small nonlinearities. In general can be said that both modes agree quite well for elastic cases despite the different formulation of respective elastic models. The viscoplastic solution for a value of $\eta = 10^{15}$ computed with both codes is included in figure 6 as well. Can be seen that the load level reached with the two codes is similar and the results obtained approach the elastic solution. In this case Metafor behaves slighty more stiff than Sogde.

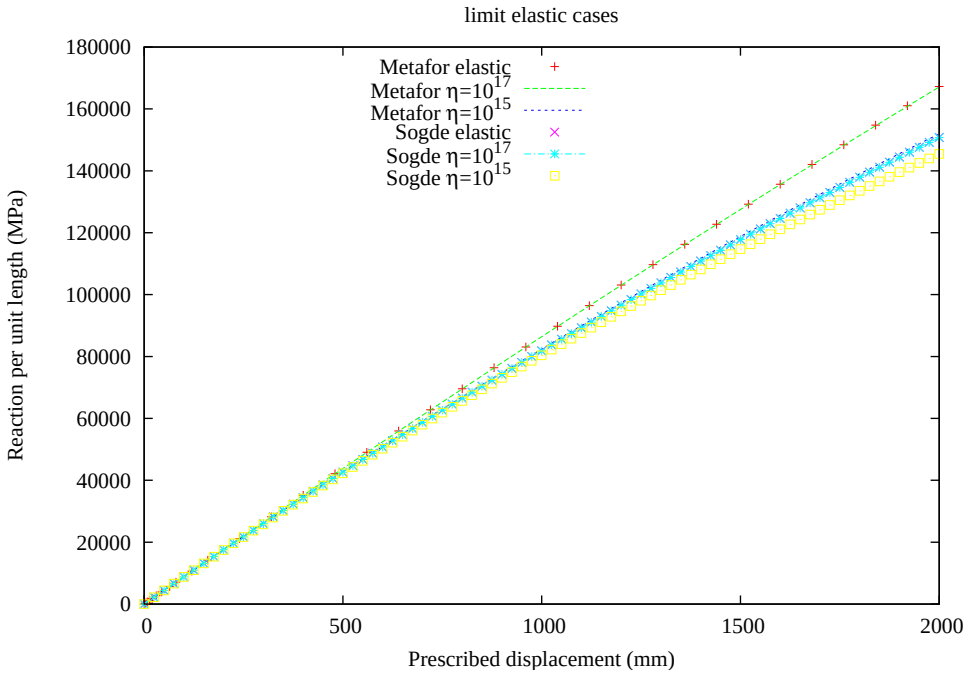


Figure 6: *load vs displacement histories for limiting elastoplastic case*

For the large strain studies carried out can be said that both codes approach rather well the limit elastic and elastoplastic cases, and the results obtained with Metafor and Sogde show a quite good agreement.

In order to study intermediate cases that behaves quite similar to elastoplastic solution, viscoplastic solution were obtained with the two codes for for a range of values of viscosity parameter $\eta$ equal to $10^2; 10^{10}; 10^{11}; 2.10^{11}; 5.10^{11}$and$10^{12}$. The obtained results are shown in figure 7 where can be seen that load-displacements histories show softening response in practically all the cases. However the load level observed depends on the viscosity considered and for $\eta = 10^12$ the limit load reaches $4500$ Mpa, while for the elastoplastic solution it is about $1400$ Mpa. From a qualitative point of view Metafor and Sogde show similar responses, but Sogde behaves stiffer than Metafor.

Copyright © 2006 Asociación Argentina de Mecánica Computacional http://www.amcaonline.org.ar

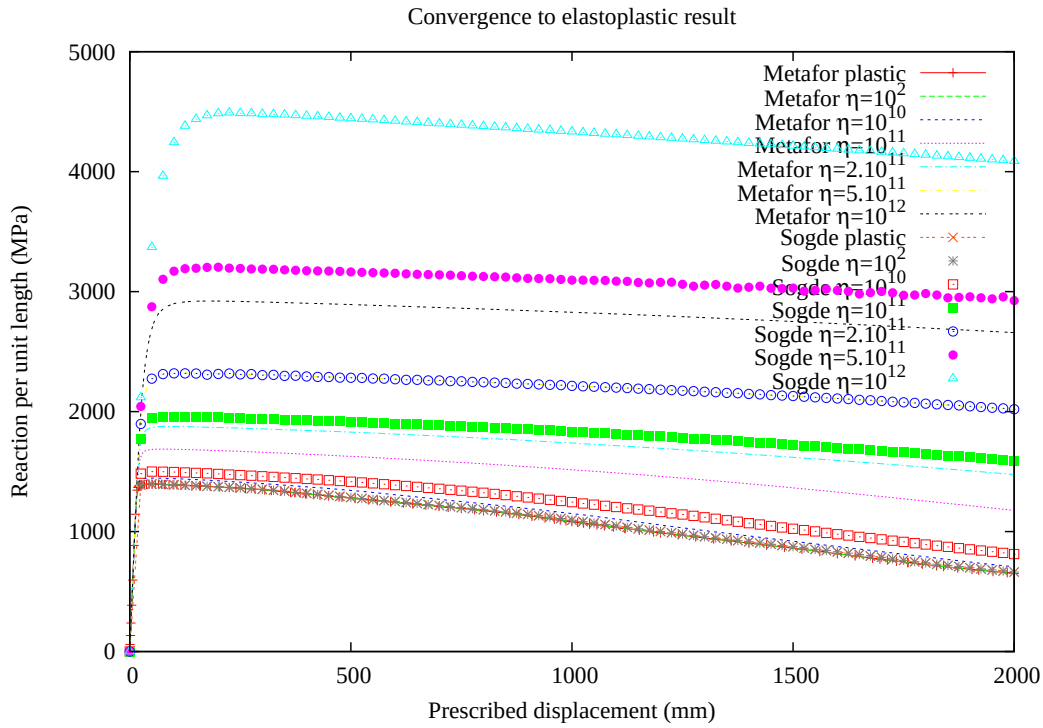


Figure 7: *Convergence to elastoplastic case: load vs displacement histories*

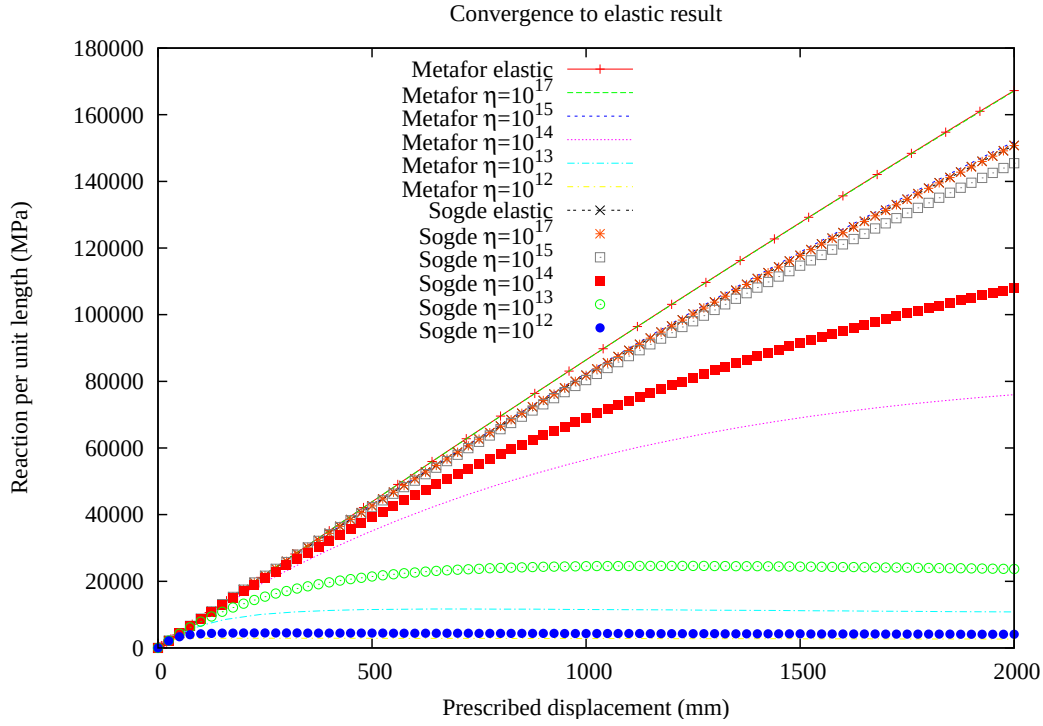


Figure 8: *Convergence to elastic case: load vs displacement histories*

Copyright © 2006 Asociación Argentina de Mecánica Computacional http://www.amcaonline.org.ar

A comparative study of viscoplastic solutions approaching the limit elastic case can be seen in 8, where the load-displacements histories computed with both codes can be seen. The range of values of viscosity parameter $\eta$ tested was: $10^{17}; 10^{15}; 10^{14}; 10^{13}$and$10^{12}$. Again in this case the behaviour of both codes is qualitative similar. For the lower values of $\eta$, $10^{12}$and$10^{13}$, the behaviour is quite similar to the *elastoplastic processes* discussed in 7. For all the other cases global hardening behaviour is found. For the larger values of $\eta$, $1.\ 10^{15}$and$1.10^{17}$ Metafor behaves slighty stiffer than Sogde, however for lower values of viscosity this effect is inverse.

For the intermediate range of viscosity values tested, $10^{10}$–$10^{14}$ Sogde show a stiffer behaviour than Metafor, result that merit a further research. In the small strain case, when the same load program was used this effect was not found. In this case different load programs where used and perhaps velocity of load could be addressed as a possible explanation. In general a rather qualitative agreement was found for both codes or the complete range of viscosity values tested, in despite of numerical differences in the load level attained.

In figure 9 a comparison of deformed shapes for the different viscoplastic cases studied is shown. Two kind of deformatios patterns can be observed. For the lower values of $\eta$ a necking type deformed shape is found in presence of large deformations in the bottom elements. In this case the marked reduction of the section near the symmetry line explains the load displacements curve found. This case could suggest a redesign of the mesh in the zone near the circular central hole.

For intermediate and greater values of $\eta$ the final deformed shape is rather similar to the elastic case and not very large strains appears to be observed. In further studies it could be usefull to compute an appropiate norm of strains for all the cases tested. For the elastic limit case can be seen that the originally circular hole takes an elliptic shape for the final configuration.

## 7 CONCLUSIONS

From the codes point of view it is worthwhile to mention that the model has been implemented and tested in Sogde. In this case the structure of elastoplastic model based on hyperelasticity and internal variables theory is mantained and viscoplastic problem is easily taken into account due the uncoupled structure of free energy function. Consequently the structure of the numerical scheme is preserved, the elastic problem remains with no changes and viscoplastic corrector step ecompass in the structure of plastic corrector when stress update algorithm is recasted in terms of kinematics variables. In this way the numerical format of the problem naturally includes viscoplasticity.

Both codes use the same stress update procedure, that is easily solved after a local non linear iterations at integration point level for the general case and various closed forms expresions are derived for different particular cases. The discussed procedure recovers the results of radial return algorithm for the inviscid case. Consequently all the advantages that can be obtained from radial return method like simplicity, robustness and computational efficiency are mantained.

Despite the different elastic models included in Metafor and Sogde results obtained are very similar. The viscoplastic model is quite simple to implement and has been included in the framework of an hyperelasticity based large strain elastoplastic model available in Sogde without difficulties.

For small strain case results obtained with both codes are practically identical. The limit elastic and elastoplastic cases are recovered for low and large values of viscosity parameter considered. No difficulties in the rate of convergence were found with any of the codes tested, for the different values of viscosity considered.

For large strain case both codes recover very well the elastic and elastoplastic limits. For

Copyright © 2006 Asociación Argentina de Mecánica Computacional http://www.amcaonline.org.ar

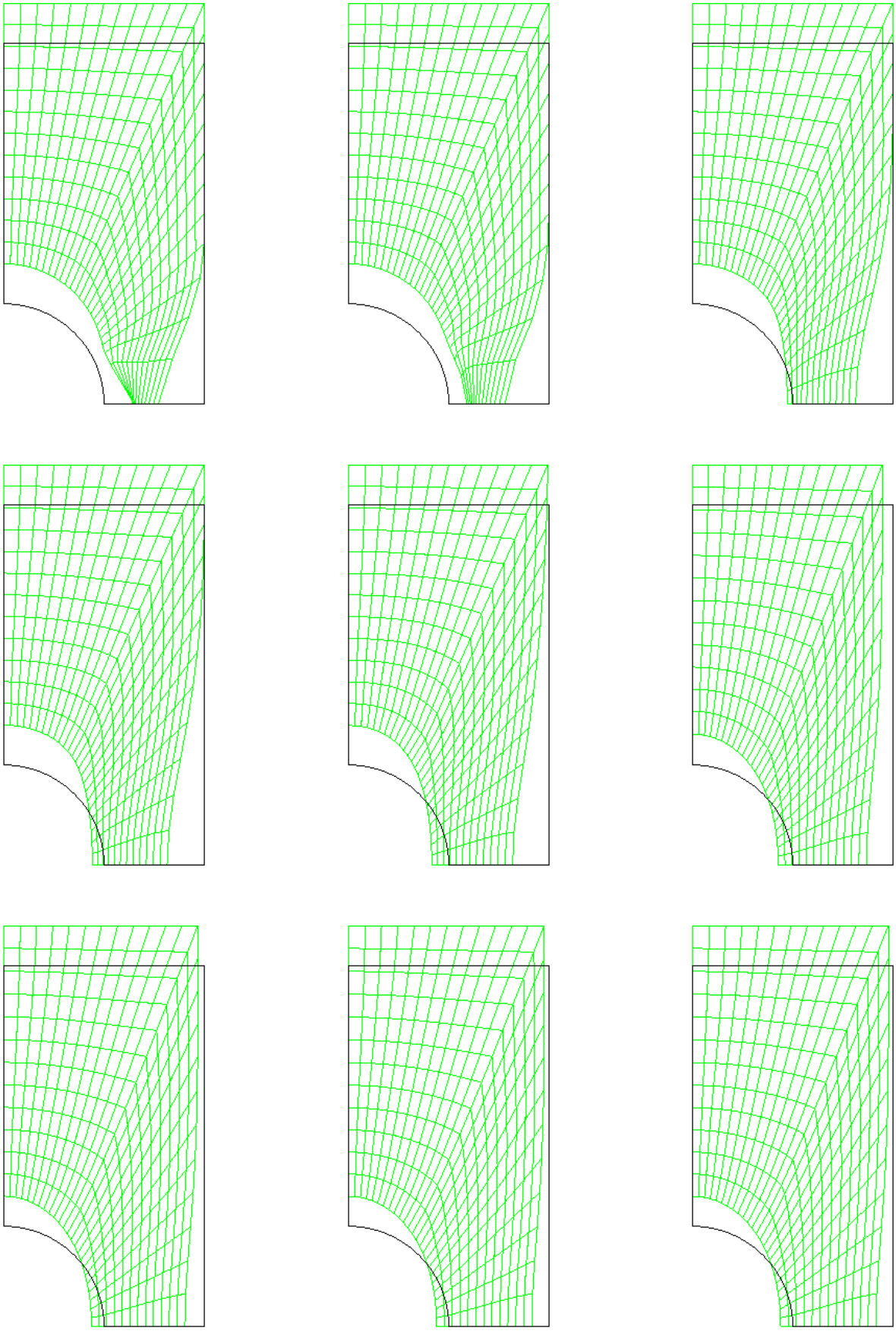

Figure 9: *Comparison of deformed shapes for different cases tested*

Copyright © 2006 Asociación Argentina de Mecánica Computacional http://www.amcaonline.org.ar

this case practically no differences are found in the results obtained with Sogde and Metafor. In the case of elastic limit both codes behave in a good agreement with the respective elastic models included, but not very different response it is found. For intermediate values of viscosity parameter differences are found in the load level attained with both codes. In general Sogde show a stiffer response than Metafor. However qualitative results are similar.

For rather low values of viscosity parameter a global softening response is obtained with both codes due to a reduction of the section in the central zone the plate. This effect can be clearly seen for the limit elastoplastic case where large strain are found in the final configuration of the body, and perhaps a mesh redesign could be necessary for this problem. In general for intermediate and larger values of viscosity considered in this work large displacements are found, but not very large stains can be observed in the deformed shape.

The differences found in the load level attained with the two codes for intermediate values of viscosity deserve further study of the problem. As a preliminary cause of this results perhaps load velocity effects can be addresed. This opinion is suggested because no differences were found for small strain case were the same program of load was used in both codes. However for large strain case different load programs were used.

## 8 ACKNOWLEDGEMENTS

Financial support from International Cooperation Project BE/PA04-EXII/003 *Comparative study of constitutive models and numerical simulation of elasto/viscoplastic large strain solids* granted by SECyT in Argentine and FNRS in Belgium and PICTR 184 Project from ANPCyT in Argentine is gratefully acknowledged.

## REFERENCES

G. Alfano, F. De Angelis, and L. Rosati. General solution procedures in elasto/viscoplasticity. *Computer Methods in Applied Mechanics and Engineering*, 190:5123–5147, 2001.

O.T. Bruhns and U. Rott. A viscoplastic model with a smooth transition to describe rate-independent plasticity. *International Journal of Plasticity*, 10(4):347–362, 1994.

A. Carosio. *Viscoplasticidad Continua y Consistente*. PhD thesis, Universidad Nacional de Tucumán, Argentina, 2001.

A. Carosio, K. Willam, and G. Etse. On the consistency of viscoplastic formulations. *International Journal of Solids and Structures*, 37:7349–7369, 2000.

C. García-Garino. *Un modelo numérico para el análisis de sólidos elastoplásticos sometidos a grandes deformaciones*. PhD thesis, E.T.S. Ingenieros de Caminos. Universidad Politécnica de Catalunya, Barcelona, 1993.

C. García Garino and J. Oliver. Un modelo constitutivo para el análisis de sólidos elastoplásticos sometidos a grandes deformaciones: Parte i formulación teórica y aplicación a metales. *Revista Internacional de Métodos Numéricos para Cálculo y Diseño en Ingeniería*, 11:105–122, 1995.

C. García Garino and J. Oliver. Un modelo constitutivo para el análisis de sólidos elastoplásticos sometidos a grandes deformaciones: Parte ii implementación numérica y ejemplos de aplicación. *Revista Internacional de Métodos Numéricos para Cálculo y Diseño en Ingeniería*, 12:147–169, 1996.

J.C. Golinval. *Calculs par éléments finis de structures élasto- viscoplastiques soumises à des chargements cycliques à haute température (in French)*. PhD thesis, University of Liège, Liège, Belgium, 1988.

Copyright © 2006 Asociación Argentina de Mecánica Computacional http://www.amcaonline.org.ar

T.J.R. Hughes. Numerical implementation of constitutive models: Rate-independent deviatoric plasticity. In S. Nemat-Nasser, R.J. Asaro, and G.A. Hegemier, editors, *Theoretical Foundation for Large-Scale Computations of Nonlinear Material Behavior*. M. Nijhoff, 1983.

T.J.R. Hughes and R.L. Taylor. Unconditionally stable algorithms for quasi - static elasto/visco - plastic finite element analysis. *Computer and Structures*, 8:169–173, 1978.

E.H. Lee. Elastic-plastic deformation at finite strains. *Journal of Applied Mechanics*, 36:1–6, 1969.

J. Lubliner. *Plasticity Theory*. Macmillan Publishing Company, 1990.

E.J. Marsden and T.J.R. Hughes. *Mathematical Foundations of Elasticity*. Prentice-Hall, 1983.

N. Ottosen and M. Ristinmaa. *The Mechanics of Constitutive Modelling*. Elsevier, 2005.

W.F. Pan. Endochronic simulation for finite viscoplastic deformation. *International Journal of Plasticity*, 13(6-7):571–586, 1997.

P. Perzyna. Fundamental problems visco-plasticity. In G. Kuerti, editor, *Advances in Applied Mechanics*, volume 9, pages 243–377. Academic Press, 1966.

P. Perzyna. Thermodynamic theory of plasticity. In Chia-Shun Yih, editor, *Advances in Applied Mechanics*, volume 11, pages 313–355. Academic Press, 1971.

J.-P. Ponthot. Unified stress update algorithm for the numerical simulation of large deformation elasto-plastic and elasto-viscoplastic processes. *International Journal of Plasticity*, 18:91–126, 2002.

J.-P. Ponthot, C. García Garino, and A. Mirasso. Large strain elastoplastic constitutive model. theory and numerical scheme. In A. Larrateguy, editor, *Mecánica Computacional*. AMCA, 2005.

J.P. Ponthot. *Traitement unifié de la Mécanique des Milieux Continus solides en grandes transformations par la méthode des éléments finis*. PhD thesis, University of Liège, Liège, Belgium, 1995.

M.B. Rubin. On the treatment of elastic deformation in finite elastic-viscoplastic theory. *International Journal of Plasticity*, 12(7):951, 1996.

J.C. Simó. A framework for finite strains elastoplasticity based on maximum plastic dissipation and the multiplicative decomposition. part i: Continuum formulation. *Computer Methods in Applied Mechanics and Engineering*, 66:199–219, 1988a.

J.C. Simó. A framework for finite strains elastoplasticity based on maximum plastic dissipation and the multiplicative decomposition. part ii: Computational aspects. *Computer Methods in Applied Mechanics and Engineering*, 68:1–31, 1988b.

J.C. Simó and M. Ortiz. A unified approach to finite deformation analyisis based on the use of hyperelastic constitutive equations. *Computer Methods in Applied Mechanics and Engineering*, 49:222–235, 1985.

J.C. Simo and T.J.R. Hughes. *Computational Inelasticity*. Springer Verlag, 1998.

I. Suliciu. Energy estimates in rate-type thermo-viscoplasticity. *International Journal of Plasticity*, 14(1-3):227–244, 1998.

C. Truesdell and W. Noll. The nonlinear field theories of mechanics. In S. Flugge, editor, *Handbuk der Physik*, volume Band III/3. Springer-Verlag, 1965.

W. M. Wang and L. J. Sluys. Formulation of an implicit algorithm for finite deformation viscoplasticity. *International Journal of Solids and Structures*, 37:7329–7348, 2000.

Copyright © 2006 Asociación Argentina de Mecánica Computacional http://www.amcaonline.org.ar